Cancer Immunology, Immunotherapy (2023) 72:903–916
https://doi.org/10.1007/s00262-022-03300-7

RESEARCH

ZIM3 activation of CCL25 expression in pulmonary metastatic nodules of osteosarcoma recruits M2 macrophages to promote metastatic growth

Jing Li[1] · Chenguang Zhao[2] · Dong Wang[1] · Shuang Wang[3] · Hui Dong[4] · Difan Wang[5] · Yubing Yang[1] · Jiaxi Li[1] · Feng Cui[1] · Xijing He[1] · Jie Qin[1]

Received: 25 March 2022 / Accepted: 20 September 2022 / Published online: 26 September 2022

Abstract

Tumor-associated macrophages (TAMs) play an important role in tumor growth and metastasis. However, the involvement of TAMs infiltration in pulmonary osteosarcoma (OS) metastasis remains poorly understood. Therefore, the effect of OS cells on macrophages migration was investigated by in vivo and in vitro experiments to evaluate the infiltration and mechanism of TAMs in pulmonary OS metastases. The results showed that the zinc finger protein ZIM3 was upregulated in OS cells than in osteoblasts and activated the expression of CCL25, which subsequently promoted the migration of M2 macrophages. *CCL25* or *ZIM3* silencing in OS cells inhibited the infiltration of M2 macrophages and the formation of pulmonary metastatic nodules in a mouse model of pulmonary OS metastasis and prolonged the survival of the mice. Furthermore, bioinformatics analyses revealed that CCL25 and ZIM3 expressions are negatively correlated with the prognosis of OS patients. In conclusion, this study found that a large number of M2 TAMs were recruited into pulmonary metastatic nodules of OS through the activation of the ZIM3-CCL25 axis in OS cells, thereby facilitating OS metastasis. Therefore, the suppression of ZIM3-CCL25-induced recruitment of M2 TAMs to the metastatic sites might be considered as a therapeutic approach to inhibit the growth of pulmonary OS metastases.

Keywords Osteosarcoma · M2 macrophages · Migration · CCL25 · ZIM3

Introduction

As the most common primary malignant bone tumor in children and adolescents, the incidence of osteosarcoma (OS) reaches 0.2–3/100,000 per year worldwide [1]. Approximately 10–20% of OS patients show metastases at the time of initial diagnosis, mainly to the lung (85–90%), occasionally to the bone (8–10%), and rarely to the lymph nodes [2]. The current treatment strategy for osteosarcoma is neoadjuvant chemotherapy followed by resection. Under this treatment strategy, patients with metastasis or recurrence still have a poor prognosis, with a 5-year survival rate of less than 20% [3]. Metastasis is one of the major causes of poor prognosis in OS patients [4]. However, the colonization and survival of at the site of metastasis remains a mystery, and a study of the factors promoting OS metastasis is urgently needed in order to design targeted and effective treatment strategies.

The tumor microenvironment (TME) is a multi-cellular ecosystem composed of many cell types, such as fibroblasts,

Jing Li and Chenguang Zhao have contributed equally to this work.

✉ Xijing He
xijing_h@vip.tom.com

✉ Jie Qin
icyhawk@163.com

1 Department of Orthopedics, The Second Affiliated Hospital of Xi'an Jiaotong University, Xi'an, Shaanxi Province, People's Republic of China

2 Department of Rehabilitation Medicine, Xijing Hospital, Fourth Military Medical University, Xi'an, Shaanxi Province, People's Republic of China

3 Institute of Photonics and Photon-Technology, Northwest University, Xi'an, Shaanxi Province, People's Republic of China

4 Department of Orthopedics, Xijing Hospital, Fourth Military Medical University, Xi'an, Shaanxi Province, People's Republic of China

5 School of Life Science and Technology, Xidian University, Xi'an, Shaanxi Province, People's Republic of China

tumor, immune, and epithelial cells [5–7]. Tumor-associated macrophages (TAMs) are among the most important immune cells, with functions such as migration and secretion of cytokines and growth factors [8, 9]. Depending on the microenvironment they embed in, TAMs can polarize into two distinct subtypes, M1-like TAMs (abbreviated as M1) and M2-like TAMs (abbreviated as M2), which exert opposite effects through the direct contact with tumor cells or by secreting different cytokines. The interaction between TAMs and tumor cells influences the phenotype and function of macrophages, as well as tumor formation and progression [10–13]. Huang et al. reported a distinct pattern in the spatial distribution of TAMs in tumors. M1 TAMs (CD68 + IRF8 + TAMs) are mainly present in the central region of a tumor mass, and this abundance is associated with necrosis in this region, whereas M2 TAMs (CD68 + CD163 + CD206 + TAMs) are abundant in the peripheral region, and this localization pattern contributes to the metastatic invasion of tumors [14].

Multiple studies showed that the number of macrophages in tumors is correlated with poor prognosis in cancer patients, and most of these macrophages are in the M2 phenotype [15–17]. M2 TAMs act as cellular chaperones for tumor cells, promote angiogenesis and tumor growth, and facilitate the metastatic cascade. Numerous studies showed that TAMs-derived cytokines and chemokines, such as CCL5 [18, 19], CXCL1 [20, 21], IL-10 [22], transcription factors [23], long non-coding RNA (lncRNAs) [24], and exosomes [25, 26], induce the epithelial–mesenchymal transition (EMT) of tumor cells and contribute to tumor metastasis and invasion. Similarly, tumor-derived cytokines and chemokines, such as CCL2 [27, 28], CCL5 [29], and CXCL12 [30], can recruit TAMs, establish the niches for metastasis, and promote the colonization and growth of metastatic tumor cells in the target organs. However, little is known on the involvement of OS cells in TAMs recruitment.

After the discovery of a massive increase of M2 TAMs in the lung of a pulmonary OS metastasis model, our in vivo and in vitro experiments revealed a putative mechanism consisting of OS cells recruiting M2 TAMs, thereby providing a research platform to study the mechanism of pulmonary OS metastasis.

Methods

Cell culture, treatments, and lentiviral infection

The OS cell lines (U2OS, 143B, MG-63 and HOS) and hFOB1.19, THP-1, and HEK293T cells (American Type Culture Collection, ATCC) were cultured in Dulbecco's modified Eagle medium (DMEM, Gibco) with 10% fetal bovine serum (FBS, Gibco) and incubated at 37 °C (hFOB1.19 cells at 33.5 °C) under 5% CO_2. The culture supernatants of OS and hFOB1.19 cells were collected and centrifuged at 4000 rpm for 10 min, filtered through a 0.22 μM filter (Merck Millipore) to remove dead-cell debris, and stored at − 80 °C to preserve their biological activity. THP-1 monocytes were treated with 100 ng/mL PMA (Abcam) for 48 h to convert them into inactivated macrophages, which were then incubated with 20 ng/mL IL-4 (Peprotech) for 48 h to obtain M2 macrophages. As regard the wound-healing assay and transwell migration assay, a CCL25-neutralizing antibody (ThermoFisher) or recombinant human CCL25 protein (rCCL25, 500 nM, Peprotech) was added into OS culture supernatants, which were then used to treat M2 macrophages to investigate the effects of the antibody and rCCL25 on the migration of the macrophages.

CCL25 (Accession Number: NM_001201359.2) and *ZIM3* (Accession Number: NM_052882.1) mRNA levels were reduced using RNAi by infecting cells with lentiviruses expressing short hairpin RNAs (shRNAs) against *CCL25* and *ZIM3*, respectively, according to the transfection procedure previously described [31]. Briefly, the targeting shRNA or a negative control shRNA (shNC) with a scrambled sequence was inserted into the pLKO.1 puro plasmid (Sigma). HEK293T cells were co-transfected with the constructed plasmid and the packaging and envelope plasmids (Sigma) using the Lipofectamine 2000 transfection reagent (ThermoFisher) to generate the lentiviruses expressing shCCL25 and shZIM3. OS cells infected by these viruses were seeded into 6-well plates (1×10^6 cells per well). The infected OS cells were selected using puromycin to obtain an OS cell population with stable expression. CCL25 and ZIM3 silencing in this population was verified using RT–qPCR. The shRNA target sequences in *CCL25* (shCCL25) and *ZIM3* (shZIM3) mRNAs were the following: shCCL25, forward oligo: 5′-CCGGGGATGCTCGAAATAAGGTTCTCGAGAACCTTATTTCGAGCATCCTTTTTG-3′, reverse oligo: 5′-AATTCAAAAAGGATGCTCGAAATAAGGTTCTCGAGAACCTTATTTCGAGCATCC-3′; shZIM3, forward oligo: 5′-CCGGGCAGAGGAAAGGCCCTATAAACTCGAGTTTATAGGGCCTTTCCTCTGCTTTTTG-3′, reverse oligo: 5′-AATTCAAAAAGCAGAGGAAAGGCCCTATAAACTCGAGTTTATAGGGCCTTTCCTCTGC-3′.

Animal ethics statement and metastatic model

Four-week-old nude BALB/c mice were obtained from the Laboratory Animal Center of Xi'an Jiaotong University and housed under specific pathogen-free conditions (ventilated room, 25 ± 1 °C, 60 ± 5% humidity, 12-h light/12-h dark cycle) with free access to food and water. All the procedures were conducted in accordance with the National Institutes of Health's Guide for the Care and Use of Laboratory Animals and approved by the Laboratory Animal Care

Committee of Xi'an Jiaotong University (Protocol number: XJTULAC2018-535). Different types of cancer cells (1×10^6 cells) were injected into the tail vein of nude mice (half female and half male), and then, the mice in the clodronate group were treated with an intranasal administration of 60 μL clodronate liposome (clodronateliposomes.org) twice a week for 2 weeks to eliminate pulmonary macrophages before injection. The survival of tumor-bearing mice was analyzed, and their pulmonary metastases were extracted (Figs. 1A, 4A, and B). Each collected lung was divided into two parts for subsequent tests. Mouse TAMs were isolated from pulmonary metastases by a magnetic-activated cell sorting using F4/80 microbeads (Miltenyi Biotec GmbH) for subsequent RT-qPCR and western blot assay.

Flow cytometry analysis of pulmonary OS metastases

The fresh pulmonary metastatic nodules were removed from the nude BALB/c mice of various groups. The tissues were

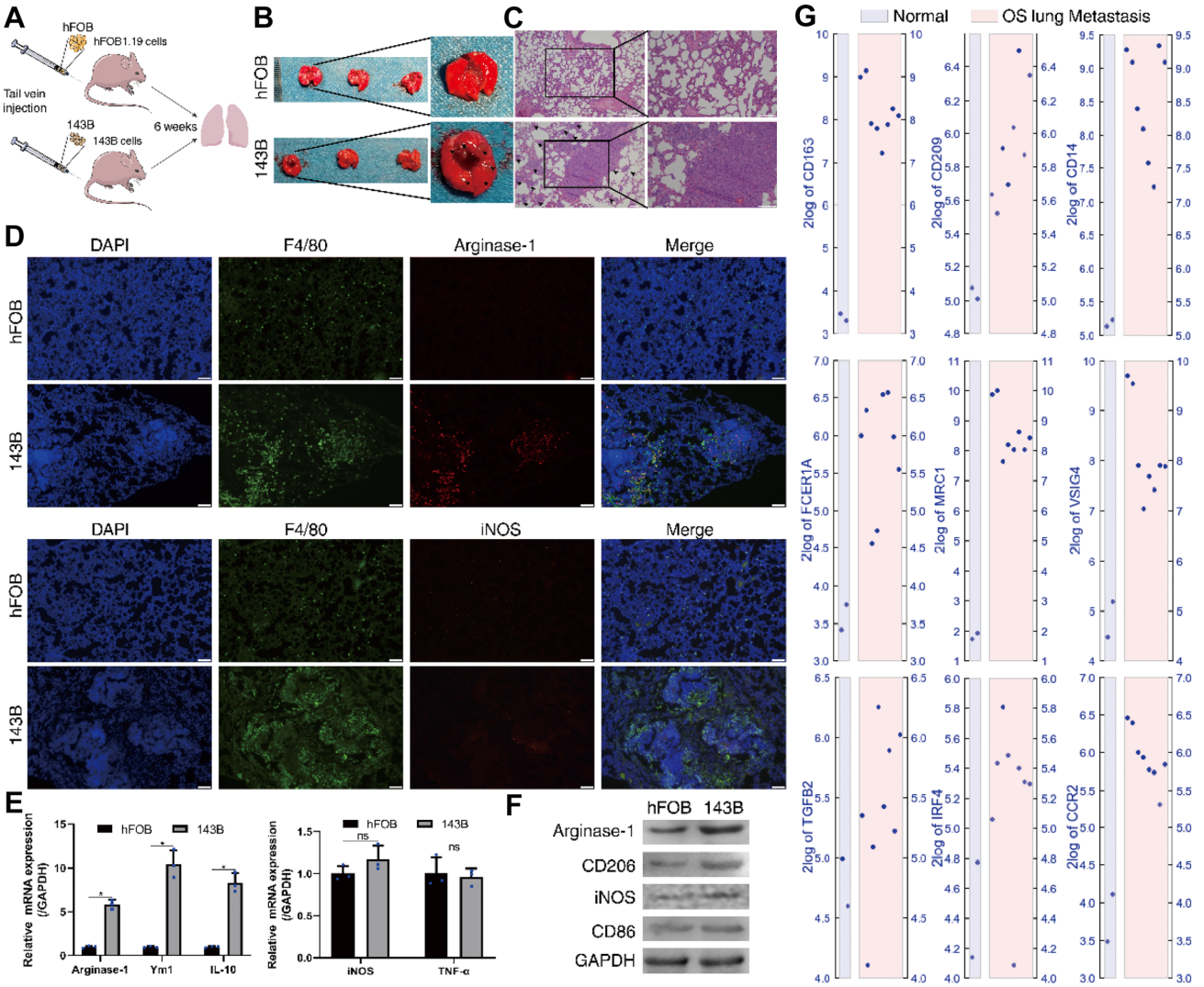

Fig. 1 M2 macrophages are recruited to pulmonary OS metastases. **A** Schematic illustration of the creation of the pulmonary OS metastasis and control groups in nude mice. 143B cells were injected into the tail vein and the group was called 143B group. hFOB1.19 cells were injected into the tail vein and the group was called hFOB group. **B** Photos of the lung samples from hFOB and 143B groups. **C** HE staining of the lung samples from hFOB and 143B groups. **D** Immunofluorescence staining of F4/80 (green) alongside Arginase-1 (red) or iNOS (red) in the lung samples from the hFOB and 143B groups. **E** mRNA expression of M1 and M2 macrophage markers in TAMs isolated from pulmonary metastases ($n = 3$). **F**) Representative immunoblots showing the expression of protein markers associated with M1 and M2 macrophages in TAMs isolated from pulmonary metastases ($n = 3$). **G** Expression of M2 macrophage markers (CD163, CD209, CD14, FCER1A, MEC1, VSIG4, TGFβ, IRF4 and CCR2) in the normal tissues and OS lung metastasis from the GSE14359 dataset. Two samples of normal tissue showed a light blue background and eight samples of OS lung metastasis showed a light red background. Results are expressed as mean ± SD. $^*p < 0.05$ (scale bar: 100 μm)

minced and incubated in DMEM supplemented with 1 mg/mL collagenase IV (Sigma) and 10 mg/mL DNase I (Sigma) for 1 h at 37 °C. Afterward, the samples were filtered through 70 μm cell strainers to obtain single-cell suspensions. The cells in each suspension were counted, and their concentration was adjusted to 10^7 cells/mL. Cells were incubated with a FITC-conjugated anti-F4/80 antibody (ThermoFisher) and PE-conjugated anti-CD206 antibody (ThermoFisher) to identify the cell phenotype. The fluorescence of the cells was analyzed by flow cytometry (Beckman Coulter Cytomics FC500) and the Flowjo software (version 10.6.2).

Macrophage migration assay

THP-1 cells were seeded in 24-well plates after the induction of M2 macrophage phenotype for the wound-healing assay. A straight wound was evenly scratched in the cell monolayer using a 200-μL sterile pipette tip, and the cell debris was washed away using phosphate-buffered saline (PBS). Then, the cells undergo different treatments for 24 h. The wound area was photographed using a light microscope (Leica Microsystems CMS GmbH) and measured using ImageJ software (version 1.53, NIH, USA). The relative migration ability was calculated as follows: relative migration = cell coverage area / original scratch area.

The migration ability of M2 macrophages was further quantified using a transwell system composed of a membrane filter with 8 μm pore size (ChemoTx® Disposable Chemotaxis System, Neuro probe). THP-1-derived M2 macrophages were seeded at a density of 5×10^4 cells per well onto a membrane filter with serum-free medium, and 35 μL culture medium or various supernatants (with or without rCCL25 or CCL25-neutralizing antibody) were added into the lower chamber. The membrane filter with M2 macrophages was placed on the lower chamber and incubated for 12 h. The cells that not fully migrated from the upper chamber of the transwell filter were wiped off with a cotton swab, and the migrated cells were fixed with 4% paraformaldehyde and stained with Giemsa. The transwell membrane was photographed, and the cells on it were counted under a light microscope (Leica Microsystems CMS GmbH).

RT-qPCR

Total RNA was isolated from cells using TRIzol reagent and subsequently reverse-transcribed into cDNA by a PrimeScripTM RT reagent kit according to the manufacturer's instructions (TaKaRa). cDNA amplification was performed using a SYBR green premix kit (TaKaRa) in an ABI 7900HT Fast Real-time PCR system. The $2^{-\Delta\Delta CT}$ method was used to calculate the relative mRNA expression, and GAPDH was used as the internal control. The sequences of the specific primers were the following: CCL25 (forward: 5′-CCAAGG TGCCTTTGAAGACT-3′ and reverse: 5′-TCCTCCAGC TGGTGGTTACT-3′), ZIM3 (forward: 5′-AACCACCAA ACCCGATGTGAT-3′ and reverse: 5′-ACTTCTCTTGCG AGACTCTCTT-3′), Arginase-1 (forward: 5′-CTGGGG ATTGGCAAGGTGAT-3′ and reverse: 5′-CAGCCCGTC GACATCAAAG-3′), Ym1 (forward: 5′- TTTCTCCAGTGT AGCCATCCTT-3′ and reverse: 5′-AGGAGCAGGAATCAT TGACG-3′), IL-10 (forward: 5′- AGACACCTTGGTCTT GGAGC-3′ and reverse: 5′- TTTGAATTCCCTGGGTGA GA-3′), iNOS (forward: 5′-AGCTCGGGTTGAAGTGGT ATG-3′ and reverse: 5′-CACAGCCACATTGATCTCCG-3′), TNF-α (forward: 5′- GGTCTGGGCCATAGAACTGA-3′ and reverse: 5′-CAGCCTCTTCTCATTCCTGC-3′), and GAPDH (forward: 5′-CCTCGTCCCGTAGACAAAATG-3′ and reverse: 5′-TGAGGTCAATGAAGGGGTCGT-3′).

Western blot analysis

Cell and tissue samples were lysed using RIPA lysis buffer (Sigma), and the total protein concentration was quantified using a NanoDrop spectrophotometer. The proteins in the lysate were denatured by boiling and then resolved using sodium dodecyl sulfate–polyacrylamide gel electrophoresis (SDS-PAGE, BioRad Laboratories). The protein bands were transferred onto a polyvinylidene fluoride membrane (PVDF, BioRad Laboratories), which was subsequently blocked with 5% BSA, followed by incubation with primary antibodies at 4 °C overnight. Afterward, the membrane was washed and incubated with horseradish-peroxidase–conjugated secondary antibodies for 1 h at room temperature. The signals of the target proteins were developed using an enhanced chemiluminescence (ECL) plus reagent (Thermo Fisher). The antibodies (and the dilution factors) used in this study were the following: Arginase-1 (CST, 1:1000), CD206 (CST, 1:1000), iNOS (Abcam, 1:1000), CD86 (CST, 1:1000), E-cadherin (Abcam, 1:3000), N-cadherin (Abcam, 1:3000), Vimentin (Abcam, 1:1000), and GAPDH (Abcam, 1:2000) used as loading control.

Chromatin immunoprecipitation (ChIP) assay

OS cells (4×10^6) transfected with pcDNA3.1-Flag-ZIM3 were seeded in 10 cm Petri dishes. When the cells reached approximately 90% confluence, they were cross-linked with 1% formaldehyde at room temperature for 10 min, and the reaction was terminated by adding a glycine solution. The chromatin was broken down to 200–1000 bp fragments by ultrasonication. The ChIP assay was performed using a Pierce Magnetic ChIP Kit (Thermo Scientific) according to the manufacturer's instructions. Briefly, the DNA fragments were incubated overnight with an anti-Flag antibody (Sigma) or normal rabbit IgG antibody at 4 °C. The protein–DNA complexes were pulled down using ChIP-Grade Protein

A/G Magnetic Beads. The relative enrichment efficiency per group of ChIP DNA was analyzed using RT-qPCR.

Dual-luciferase reporter assay

The promoter region of the *CCL25* gene from −2000 to + 100 nt was amplified using PCR. Mutant *CCL25* promoter constructs (mut1 and mut2) were similarly generated using PCR. The PCR products containing the targeted sequence were digested and cloned into the pGL-3 Basic vector (Promega). 143B and MG-63 cells (1×10^4 cells/well) were seeded into 96-well plates and co-transfected with the CCL25 dual-luciferase reporter plasmid (pGL3-WT, pGL3-Mut1, or pGL3-Mut2) or an empty pGL-3 vector, and pcDNA-ZIM3 or an empty pcDNA vector, as well as with pRL Renilla luciferase reporter vector using Lipofectamine 3000 transfection reagent (Thermofisher) according to the manufacturer's instructions. The cells were lysed after 48 h, and the culture supernatants were collected. The firefly and Renilla luciferase activities were quantified using a Dual-Luciferase Reporter Assay System (Promega). The levels of Renilla luciferase activity were used to normalize the levels of firefly luciferase activity.

Histological analysis

Lungs were collected and fixed with 4% paraformaldehyde (Sigma) for 48 h, embedded in paraffin, and cut into 5 µm-thick sections. Hematoxylin and Eosin (HE) staining was performed according to a standard protocol. In short, sections were deparaffinized, then the nucleus and cytoplasm were stained with 10% hematoxylin and 1% eosin, respectively (Solarbio Life Sciences). The stained tissues were observed using a light microscope (Leica Microsystems CMS GmbH). As regards the immunofluorescent staining, the lungs were embedded in the optimal cutting temperature (OCT) compound (Sakura) and cut into 20 µM-thick sections. OS cells transfected with pcDNA3.1-Flag-ZIM3 on coverslips were fixed with 4% paraformaldehyde. The sections and OS cells were permeabilized with 0.3% Triton X-100 (Sigma) and blocked with 1% BSA (Sigma). Afterward, the sections and OS cells were consecutively incubated with primary and secondary antibodies, and the cell nuclei were stained with DAPI. The stained tissues and cells were observed using a conventional (Zeiss Axio Vert.A1) or confocal (Leica TCS SP8) fluorescence microscope. The antibodies (and the dilution factors) used were the following: F4/80 (CST, 1:100), Arginase-1 (CST, 1:200), iNOS (Abcam, 1:500), anti-Flag antibody (Sigma, 10 µg/mL), Alexa Fluor 488 goat anti-rat IgG (Abcam, 1:500), and Alexa Fluor 555 donkey anti-rabbit IgG (Abcam, 1:500).

Bioinformatics analysis

The GSE14359 and GSE85537 datasets were downloaded from the Gene Expression Omnibus (GEO) database (https://www.ncbi.nlm.nih.gov/gds/). The GSE14359 dataset was used to analyze the expression profiles of markers related to M2 macrophages in human normal osteoblasts *versus* pulmonary OS metastases. The GSE85537 dataset was used to identify the differentially expressed genes between primary and metastatic tumors derived from a mouse model of OS. Based on the gene expression data of GSE85537, gene set enrichment analysis (GSEA) was performed using the GSEA software (version 4.1.0). The mRNA profiling data of OS patients were downloaded from the TARGET database (https://ocg.cancer.gov/programs/target), and the correlation among genes was visualized using the ggplot2 R package. The Kaplan–Meier survival curves for overall and metastasis-free survival rates of the OS patients were plotted using the R2 database (http://r2.amc.nl), which is a genomics analysis and visualization platform. The mixed osteosarcoma-Kuijjer-127-vst-ilmnhwg6v2, Tumor Osteosarcoma-Buddingh-53-vst-ilmnhwg6v2, and Tumor Osteosarcoma-Kobayashi-27-MAS5.0-u133p2 datasets were selected for analysis. The JASPAR database (https://jaspar.genereg.net/) was used to predict the binding site(s) of the transcription factor ZIM3 in the *CCL25* promoter.

Statistical analysis

Statistical analysis was performed using SPSS 22.0 software and the results were presented as mean ± SD. Two-group and multiple-group comparisons were performed using the Student's *t* test and one-way analysis of variance (ANOVA), respectively. The Kaplan–Meier methodology and Chi-squared test were used to analyze the prognoses of OS patients or mouse models and the relationship of CCL25 expression with ZIM3 expression, respectively. Spearman's rank correlation analysis was applied to identify the differentially expressed genes in OS patients *versus* healthy individuals. A value of $p < 0.05$ was considered statistically significant.

Results

M2 macrophages are recruited to and enriched at pulmonary OS metastases

The mouse model of pulmonary OS metastasis was constructed by a tail-vein injection of 143B cells (143B group), and the control model was constructed by an injection of hFOB1.19 osteoblasts (hFOB group) (Fig. 1A). The human osteoblast cell line hFOB1.19 is often used as a model of

normal human osteoblast cells [32–34]. There was A significant pulmonary metastatic nodule formation was found in the 143B group, but not in the hFOB group (Fig. 1B and C). Immunofluorescence staining was performed to evaluate the infiltration of macrophages in pulmonary metastatic nodules. Many macrophages co-expressing Arg-1 and F4/80 around the pulmonary metastatic nodules were observed in the 143B group than in the hFOB group, and both groups had less iNOS and F4/80 double-positive macrophages than Arg-1 and F4/80 double-positive macrophages (Fig. 1D). TAMs were isolated from the lung in both groups, and the expression of the markers of M1 or M2 TAMs was measured using RT-qPCR and western blot. The mRNA and protein expression of the M2-related markers was significantly higher in the 143B group than in the hFOB group, whereas no significant difference in the expression of the M1-related markers was observed between the two groups (Fig. 1E and F). Likewise, the M2-related markers (such as CD163, CD209, CD14, FCER1A, MEC1, VSIG4, TGFβ, IRF4, and CCR2) were highly expressed in human pulmonary OS metastases in the GSE14359 dataset (Fig. 1G). The above results confirmed a significant enrichment of M2 macrophages in the pulmonary metastatic tissue of OS, while no significant increase in M1 macrophages was found.

OS cell derived CCL25 promotes the migration of M2 macrophages

The culture supernatants of 143B, MG-63, and hFOB1.19 cells were collected to treat THP-1–induced M2 macrophages to investigate whether and how OS cells promote the infiltration of M2 macrophages, and the culture medium of OS cells was used as control (CTL group). The results of the wound-healing and transwell migration assay showed that 143B and MG-63 supernatants significantly promoted the migration of M2 macrophages in vitro, compared with CTL and hFOB supernatants (Fig. 2A).

The keywords "osteosarcoma, primary tumor, and lung metastases" were used for searching the GEO database (https://www.ncbi.nlm.nih.gov/) to clarify the mechanism

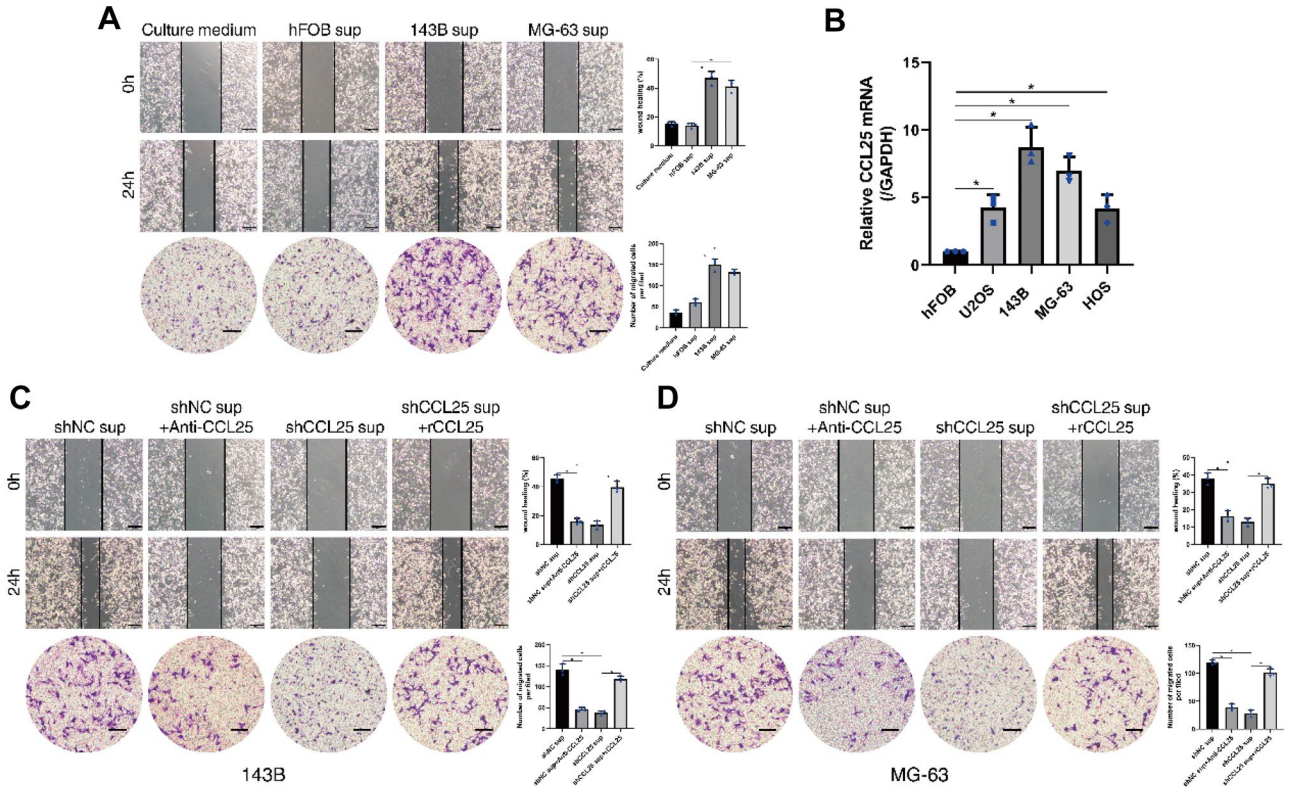

Fig. 2 OS-derived CCL25 promotes the migration of M2 macrophages in vitro. **A** Wound healing (scale bar: 200 μm) and transwell (scale bar: 100 μm) assays on M2 macrophages treated with various cell culture supernatants. **B** *CCL25* mRNA expression relative to *GAPDH* mRNA expression in various human OS cell lines ($n=3$). **C)** 143B cells were transfected with a negative-control shRNA (shNC) or a targeting CCL25 shRNA (shCCL25), and the supernatants were collected. The wound-healing and transwell assays were performed on M2 macrophages treated with 143B-cell supernatant supplemented with a CCL25-neutralizing antibody or recombinant CCL25 protein. **D)** MG-63 cells were transfected with shNC or shCCL25, and the supernatants were collected. The wound healing and transwell assays were performed on M2 macrophages treated with MG-63–cell supernatant supplemented with a CCL25-neutralizing antibody or recombinant CCL25 protein. Results are expressed as mean ± SD. *$p<0.05$

used by OS cells to promote M2 macrophage migration and 21 datasets were consequently collected. Among these datasets, our attention was mainly focused on GSE85537, which contains gene expression data from mouse pulmonary OS metastases and bone primary OS tumors. Subsequently, GSE85537 was analyzed to screen the differentially expressed genes associated with pulmonary metastasis in the OS model. The gene expression in the primary and pulmonary metastatic tumors was compared using the volcano plot, and the most significantly up- or downregulated genes were presented by a cluster heat map (Fig. S1A and B). Gene set enrichment analysis (GSEA) based on the gene expression data of GSE85537 indicated that the CCL25 high expression group was associated with cadherin-mediated cell adhesion (Fig. S1C). The expression of CCL25 was significantly higher in the pulmonary OS metastases than in the primary tumors (Fig. S1D). Then, RT-qPCR was performed to examine CCL25 expression in hFOB1.19 cells and various OS cell lines, and the results showed that OS cells, especially 143B and MG-63 cells, had a higher and significant expression of CCL25 than hFOB1.19 cells (normal osteoblasts) (Fig. 2B). Our hypothesis was that CCL25 played an important role in the promotion of M2 macrophage migration induced by OS cells. Indeed, shRNA-induced silencing of CCL25 expression or the addition of a CCL25-neutralizing antibody inhibited the ability of the OS cell-culture supernatant to promote M2 macrophage migration. However, the addition of rCCL25 into the shCCL25 supernatant rescued the migration ability of M2 macrophages (Fig. 2C–D). The above results suggested that OS cells promoted M2 macrophage migration through CCL25.

CCL25 expression in OS cells is activated by ZIM3

Among the genes upregulated in the pulmonary metastatic tumor group of the GSE85537 dataset, a protein-coding gene, *ZIM3*, also known as *ZNF264* or *ZNF657*, was identified. ZIM3 was significantly increased in OS cells (Fig. S1D), and RT-qPCR confirmed this result (Fig. 3A). The Spearman correlation analysis showed that the expression of CCL25 and ZIM3 was positively correlated in the tissues of the OS patients in the TARGET database (Fig. 3B). Our speculation was that ZIM3 might be involved in the transcriptional regulation of *CCL25* in OS cells. Two potential binding sites (P1 and P2) for ZIM3 in the *CCL25* promoter were predicted using an online bioinformatics tool (http://jaspar.genereg.net) (Fig. 3C). The immunofluorescence assay showed that ZIM3 was localized in the nuclei of 143B and MG-63 cells, and confirmed that ZIM3 expression was lower in hFOB1.19 cells than in 143B or MG-63 cells (Fig. 3D). shRNA-induced knockdown of *ZIM3* also downregulated CCL25 in 143B and MG-63 cells (Fig. 3E and D). The ChIP assay and dual-luciferase reporter assay were performed to investigate whether ZIM3 transcriptionally regulated *CCL25*. The ChIP assay results suggested that ZIM3 directly bound to the CCL25 promoter in the human OS cell lines (Fig. 3F). The CCL25 promoter region (WT) and two mutant sequences (Mut1 and Mut2) were cloned into the luciferase reporter plasmid (Fig. 3G). The luciferase activity of the WT and Mut1 luciferase reporter plasmids were significantly induced by ZIM3 in 143B and MG-63 cells, unlike that of the Mut2 luciferase reporter plasmid in OS cells. This result revealed that ZIM3 bound to the P2 region located 125 nt upstream of *CCL25*. Furthermore, shRNA-induced knockdown of *ZIM3* in OS cells significantly inhibited the pro-migratory effect of the culture supernatant of OS cells on M2 macrophages (Fig. 3H). The above results confirmed that the increased expression of ZIM3 in the nucleus of OS cells activated the transcriptional regulation of CCL25 and that the CCL25-ZIM3 axis promoted the migration of M2 macrophages in vitro.

OS-derived CCL25 recruits M2 macrophages to form a pulmonary metastatic environment for OS in vivo

In vivo pulmonary metastatic tumor models were constructed by injecting various 143B cells with or without clodronate liposomes into nude mice (Fig. 4A and B) to verify the role of CCL25 and ZIM3 in the recruitment of M2 macrophages to pulmonary OS metastases. the survival of the 6 mice in each group was monitored for 8 weeks, and the results showed that the shCCL25 group, shZIM3 group, and the Clodronate group significantly prolonged the survival of the mice compared with that in the shNC group (Fig. 4A). Furthermore, lung samples from another set of 6 mice were collected at 4 weeks post-injection (Fig. 4B). Pulmonary metastases in the shNC group possessed the largest volume and were more numerous than those in other groups (Fig. 4B and C). shCCL25 and shZIM3 groups had significantly less Arg-1–positive M2 macrophages infiltrated in the pulmonary metastases than the shNC group (Fig. 4D). Clodronate liposomes were used to eliminate alveolar macrophages and the clodronate-liposome treatment significantly reduced the number of macrophages in the mouse lung tissues and inhibited the formation of pulmonary OS metastases (Fig. 4C and D). This result was confirmed by isolating cells from the pulmonary metastases. Flow cytometry analysis showed a significantly higher proportion of CD206-positive cells among the F4/80-positive cells in the shNC group compared with shCCL25 and shZIM3 groups, and clodronate liposome significantly eliminated the F4/80-positive macrophages in the lung (Fig. 4E). Our results from western blot analysis showed that the pulmonary expression of the mesenchymal markers such as N-cadherin and vimentin was significantly higher in the shNC group than in the other groups, whereas the pulmonary expression of the epithelial marker

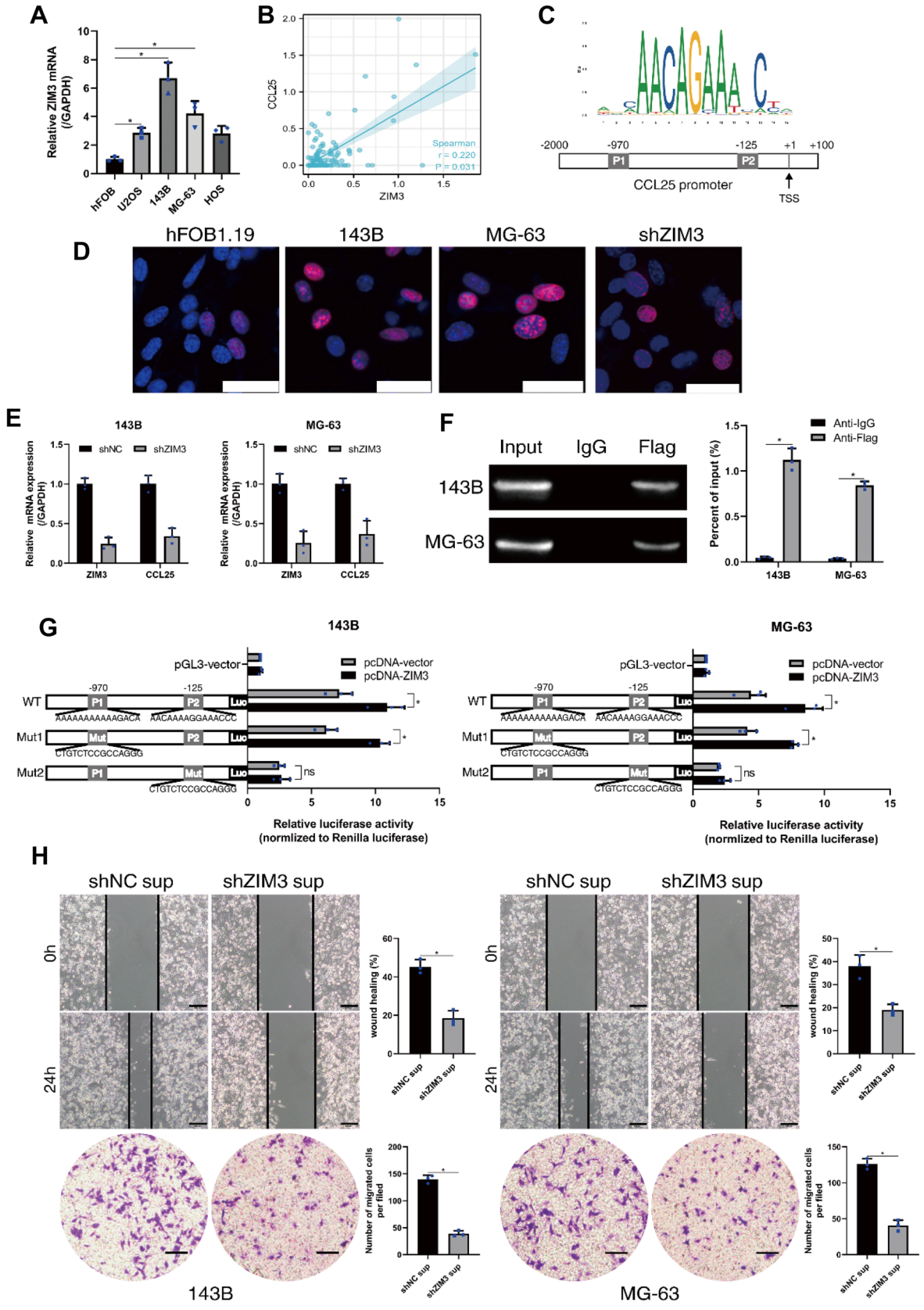
A
Relative ZIM3 mRNA (/GAPDH)
hFOB
U2OS
143B
MG-63
HOS
B
CCL25
ZIM3
Spearman
r = 0.220
P = 0.031
C
-2000
-970
-125
+1
+100
P1
P2
CCL25 promoter
TSS
D
hFOB1.19
143B
MG-63
shZIM3
E
143B
MG-63
shNC
shZIM3
Relative mRNA expression (/GAPDH)
ZIM3
CCL25
F
Input
IgG
Flag
143B
MG-63
Anti-IgG
Anti-Flag
Percent of input (%)
G
143B
MG-63
pGL3-vector
pcDNA-vector
pcDNA-ZIM3
WT
Mut1
Mut2
Luc
Mut
ns
Relative luciferase activity (normlized to Renilla luciferase)
H
shNC sup
shZIM3 sup
0h
24h
wound healing (%)
Number of migrated cells per filed
143B
MG-63

◂**Fig. 3** ZIM3 binds to the *CCL25* promoter and activates the transcription of *CCL25*. **A** Relative *ZIM3* mRNA expression normalized to *GAPDH* mRNA expression in human OS cell lines ($n=3$). **B** Spearman correlation analysis of the expression of CCL25 and ZIM3 in the TARGET database. **C** Two transcriptional binding sites of ZIM3 were predicted through an online bioinformatics tool (http://jaspar.genereg.net) for the *CCL25* promoter. **D** The subcellular localization of ZIM3 (Red) was observed using a confocal microscope (Scale bar: 25 μm). shRNA-induced knockdown of ZIM3 in 143B cells was called shZIM3 group. **E)** Expression of ZIM3 in 143B and MG-63 cells transfected with shNC or shZIM3 ($n=3$). **F** 143B and MG-63 cells were subjected to the ChIP assay to assess the ZIM3 binding to CCL25 promoter. IgG and input fractions were used as controls ($n=3$). **G** Relative luciferase activities of the OS cells (143B and MG-63 cells) with a luciferase reporter plasmid containing the wild type or mutant *CCL25* promoter ($n=3$). **H** Wound healing (Scale bar: 200 μm) and transwell (Scale bar: 100 μm) assays on M2 macrophages treated with the culture supernatant of OS cells transfected with shNC or shZIM3. Results are expressed as mean ± SD. $^*p<0.05$

E-cadherin was downregulated in the shNC group compared with the expression in the other groups (Fig. 4F). The above results confirmed that ZIM3 and CCL25 promoted the infiltration of M2 macrophages to pulmonary OS metastases, and infiltrated M2 macrophages created an environment conducive to metastasis through the stimulation of the EMT.

CCL25 and ZIM3 expression is negatively correlated with the prognosis of OS patients

Correlation analysis between the expression of CCL25, ZIM3, and the M2 macrophage marker Arginase-1 in human OS patients was performed, and the results showed that both CCL25 and ZIM3 were positively correlated with Arginase-1 in the TARGET database (Fig. 5A). In addition, the R2 database was used to analyze the effects of CCL25 and ZIM3 expression on the prognosis of OS patients. Kaplan–Meier survival curves showed that OS patients with high CCL25 or ZIM3 expression had significantly lower overall and metastasis-free survival rates (Fig. 5B). The box plot showed that the expression of CCL25 and ZIM3 was slightly higher in patients with OS metastases than in non-metastatic patients, based on the R2 database (Fig. 5C). The above bioinformatics results showed that the high expression of CCL25 or ZIM3 was associated with a high number of infiltrated M2 macrophages and poor prognosis in OS patients.

Discussion

M2 TAMs play important roles in the metastasis of malignant tumors [11]. They secrete various proteolytic enzymes that degrade the extracellular matrix (ECM) around tumor cells [35], regenerate the tumor vascular system by upregulating pro-angiogenic molecules [36], and promote tumor-cell extravasation [37], thereby establishing a suitable environment for tumor cell colonization at distant sites. In our study, the nude mice deprived of macrophages by clodronate liposome injection showed almost no pulmonary metastasis, suggesting that TAMs played a very important role in promoting pulmonary OS metastasis. Our results also showed a significantly increased IL-10 expression in TAMs isolated from pulmonary metastases, and this cytokine has been reported to promote tumor cell metastasis. Accordingly, our speculation was that the formation of pulmonary metastases in the 143B group was related to IL-10 secretion by TAMs [38, 39]. Lee et al. similarly showed that macrophages depletion by clodronate liposome significantly suppresses both primary tumor growth and pulmonary metastasis [40]. However, only few studies on how OS cells recruit M2 macrophages to metastatic sites are available.

The infiltration of non-malignant cells in primary and metastatic tumors is mainly induced by chemokines. The chemokine secretion pattern of tumor cells determines the distribution of immune cells in the TME. CC chemokines released from breast cancer, pancreatic cancer, sarcoma, and glioma induce the infiltration of macrophages and lymphocytes [41]. Geng et al. found that the auto-amplification of the Notch signaling in pancreatic cancer cells activates IL-8 and CCL2, promoting the recruitment and activation of M2 macrophages [28]. Qian et al. found that CCL2 synthesized by the tumor and stroma in breast cancer recruits CCR2-expressing inflammatory monocytes and the inhibition of the CCL2-CCR2 signaling inhibits breast cancer metastasis in vivo and prolongs the survival of tumor-bearing mice [42]. Walens et al. showed that CCL5, which is highly expressed in residual breast cancer, promotes collagen deposition in residual tumors and also tumor recurrence by recruiting CCR5-expressing macrophages. Recurrence of breast cancer can be effectively prevented by blocking the CCL5-macrophage axis [29]. Our findings showed that OS cells promoted the infiltration of many M2 macrophages in both the mouse models and patients with OS pulmonary metastases. The in vitro tests also confirmed the ability of OS cell supernatant to promote M2 macrophage migration. Our attention was focused on CCL25, which is highly expressed in OS cells, due to the important role chemokines play in macrophage recruitment. CCL25, also called thymus expressed chemokine (TECK), has chemotactic effects on dendritic cells, thymocytes, and activated macrophages. CCL25 is significantly expressed in the epithelial cells of the small and large intestine and is one of the main factors that predispose different type of cancers, such as melanoma and ovarian cancer, to metastasize the intestine [43]. Our results showed that exogenous rCCL25 promoted M2 macrophage migration, and the pro-migratory effect of the culture supernatants of OS cells was blocked by a CCL25-neutralizing antibody. Furthermore, shRNA-mediated

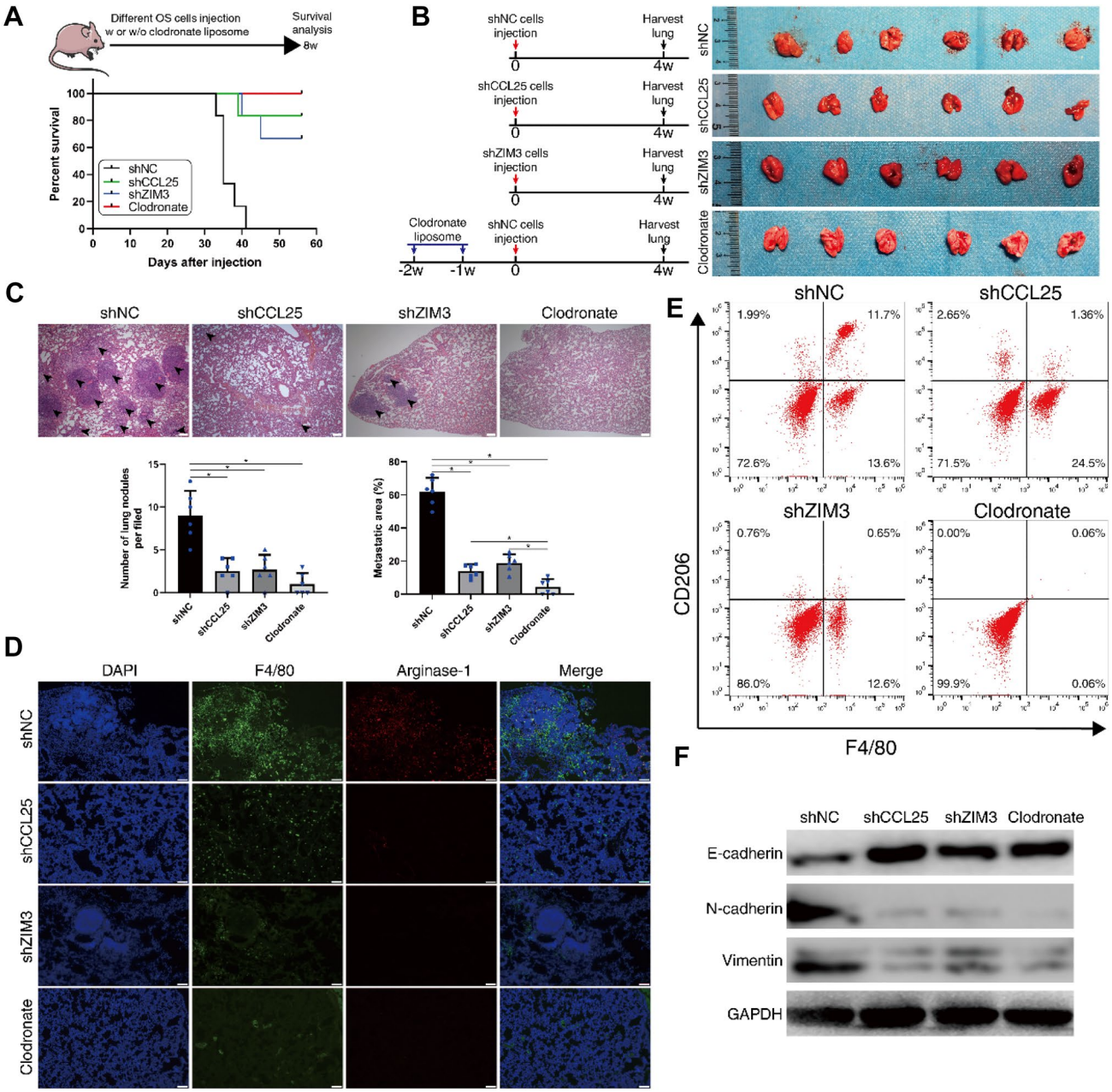

Fig. 4 CCL25 recruits M2 TAMs in vivo and promotes the pulmonary metastasis of OS. **A** Kaplan–Meier analysis of the survival of mice after the injection of 143B cells transfected with shRNA with or without clodronate liposomes ($n=6$). The experiment finished at 8th week after cell injection. shNC group (black), shCCL25 group (green), shZIM3 group (blue), Clodronate group (red). **B** Schema of the animal experiment and images of the lung samples from different groups. 143B cells ($1\times10.^{6}$ cells) were injected into the tail vein of nude mice, and the lung was harvested after 4 weeks. The nude mice in the clodronate group were treated with an intranasal administration of 60 μL clodronate liposomes twice a week for 2 weeks prior to 143B cell injection. **C** HE staining of lung samples from shNC, shCCL25, shZIM3, and Clodronate group (Scale bar: 200 μm). **D** Immunofluorescence staining of F4/80 (green) and Arginase-1 (red) in lung samples from shNC, shCCL25, shZIM3, and Clodronate group (Scale bar: 100 μm). **E** Flow cytometry analysis was used to detect CD206 and F4/80 expression in cells of pulmonary metastatic nodules (n = 3). **F** Representative immunoblots display the markers of epithelial-mesenchymal transition in the lung samples from shNC, shCCL25, shZIM3, and Clodronate group ($n=3$). Results are expressed as mean ± SD. $^{*}p<0.05$

CCL25 knockdown in OS cells inhibited the pro-migratory effect of the supernatant from OS cell culture on M2 macrophages in vitro, as well as M2 macrophage infiltration and metastatic tumor formation in vivo. The in vitro experiments by Spinnen et al. also confirmed that exogenous CCL25 promotes macrophage migration in a dose-dependent manner

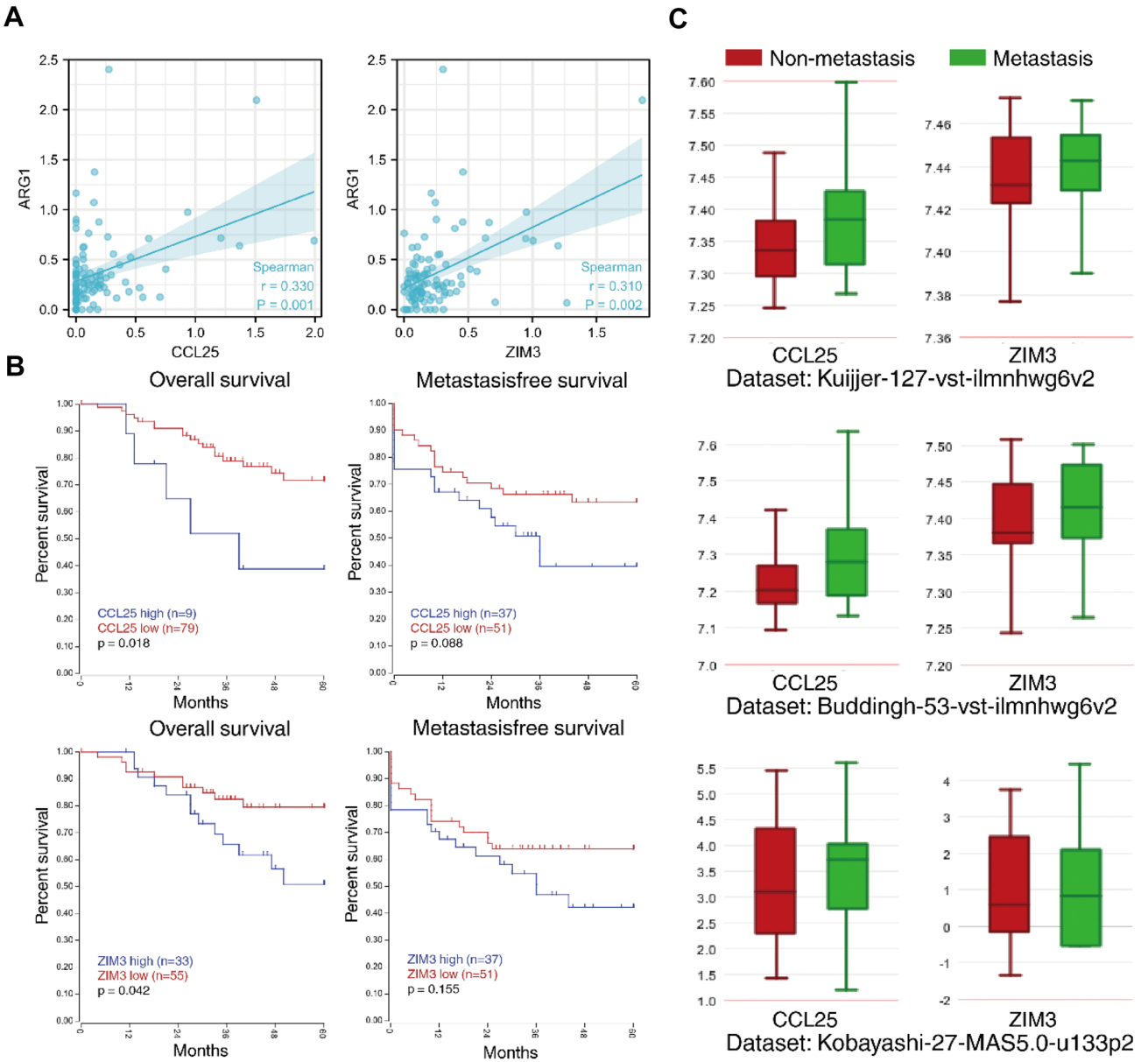

Fig. 5 Bioinformatics analysis of CCL25 and ZIM3 expression in OS patients. **A** Spearman correlation analysis between the Arginase-1 and CCL25 or ZIM3 expression reported in the TARGET database. **B** Kaplan–Meier analysis of the overall and metastasis-free survival rates of OS patients was performed based on the R2 database. The OS patients were divided into CCL25 and ZIM3 high-expression (blue) and low-expression (red) groups for comparison. **C** Expression of CCL25 and ZIM3 in patients with metastatic (green) or non-metastatic (red) OS. The expression data selected in this study were obtained from three datasets in the R2 database (the Mixed osteosarcoma-Kuijjer-127-vst-ilmnhwg6v2 dataset, Tumor Osteosarcoma-Buddingh-53-vst-ilmnhwg6v2 dataset, and Tumor Osteosarcoma-Kobayashi-27-MAS5.0-u133p2 dataset)

[44]. Several studies confirmed that chemokine receptor 9 (CCR9) and its exclusive ligand CCL25 are overexpressed in a variety of malignancies and are strongly associated with tumor proliferation, apoptosis, invasion, migration, and drug resistance [45, 46]. The CCL25/CCR9 axis promotes macrophage recruitment and fibrogenesis in a mouse model of nonalcoholic steatohepatitis [47]. In addition, CCL25/CCR9 interaction modulates the inflammatory immune response in the colonic mucosa by balancing different dendritic cell subpopulations and remodels macrophages to mature osteoclasts in rheumatoid arthritis [48, 49]. Therefore, our hypothesis was that OS cell-derived CCL25 might recruit macrophages through the CCR9 receptor. Similarly, Jacquelot et al. showed that pulmonary metastasis of melanoma is also due to the CCR9-CCL25 axis [50].

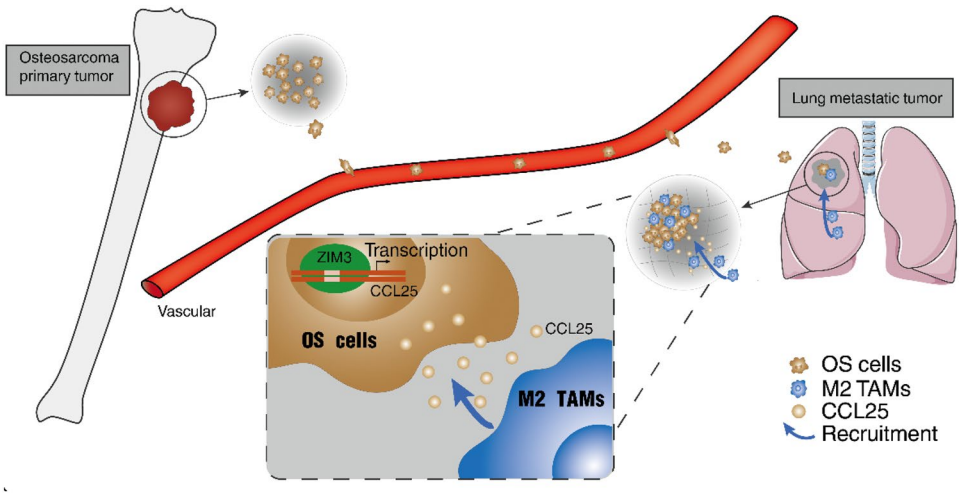

Fig. 6 Schematic illustration of the mechanism used by OS cells to recruit M2 macrophages. The upregulation of ZIM3 in OS cells activates the expression of *CCL25*, which recruits M2 macrophages to form a pro-metastatic environment in the lung

However, the mechanism that upregulates CCL25 in OS cells remains unclear. Previous studies showed that the transcription of CC chemokine ligands is regulated by zinc finger (ZNF) proteins [51–53]. ZNF proteins are a class of transcription factors with finger-like structural domains and play important roles in the regulation of gene expression. They influence tumor progression by regulating the transcription of genes involved in tumor proliferation, apoptosis, or invasion [54, 55]. Our study found that the expression of ZIM3 was significantly increased in OS cells and was positively correlated with CCL25 expression. ZIM3, also known as ZNF264 and ZNF657, is a rarely expressed zinc finger protein, which is related to nucleic acid binding and DNA-binding transcription factor activity [56]. The results of our ChIP assay and dual-luciferase reporter assay confirmed that ZIM3 directly bound to the promoter of CCL25 and activated the expression of this gene in OS cells. This result was corroborated by the result showing that CCL25 was downregulated after *ZIM3* knockdown. In addition, ZIM3 knock down inhibited the pro-migratory effect of OS cells on M2 macrophages in vitro and in vivo, and the formation of pulmonary metastases was significantly inhibited in the shZIM3 group.

Primary tumors accumulate cells derived from the marrow of distant bones, thereby increasing the efficiency of metastasis [57, 58]. Helm et al. showed that M2 TAMs downregulate E-cadherin in hepatocellular carcinoma, gastric cancer, and pancreatic ductal carcinoma, and induce the EMT of tumor cells [59]. Our analyses on the protein expression similarly showed that shCCL25 and shZIM3 significantly reduced the activation of the EMT pathway in pulmonary metastases. The survival curves of the pulmonary metastasis models in our study showed that the nude mice in the shCCL25 and shZIM3 groups survived significantly longer than those in the shNC group. Similarly, the bioinformatics analysis showed that OS patients with high expression of CCL25 or ZIM3 had a poor prognosis. Lee et al. showed that increased CCL25/CCR9 expression in pancreatic cancer patients was associated with poor prognosis [60]. However, our analysis on the survival prognosis derived only from published data without our own clinical data, which represents a limitation of this study.

In this study, ZIM3, which is overexpressed in OS cells, was found to act as a transcriptional activator of *CCL25*. Since OS cells colonize metastatic sites, OS-derived CCL25 recruits M2 macrophages, which facilitates multiple metastasis processes (Fig. 6). Consequently, the inhibition of the ZIM3-CCL25-macrophage axis reduced the enrichment of M2 macrophages at the metastatic sites and inhibited the growth of pulmonary OS metastases. Our study findings demonstrate that the blockage of ZIM3 or CCL25 might be a promising approach in the treatment of pulmonary OS metastases.

Supplementary Information The online version contains supplementary material available at https://doi.org/10.1007/s00262-022-03300-7.

Author contributions JL contributed to conceptualization, methodology, software, validation, formal analysis, investigation, writing the original draft, writing, reviewing and editing; CZ contributed to conceptualization, methodology, validation, formal analysis, writing, reviewing and editing; DW performed data curation; SW carried out formal analysis; DW contributed to investigation and resources; FC provided software; YY contributed to methodology and validation; JL contributed to formal analysis and resources; XH was involved in conceptualization, project administration, and funding acquisition; JQ contributed to conceptualization, methodology, writing, reviewing and editing, project administration, and funding acquisition.

Funding This work was supported by the Shaanxi Province Innovation Talent Promotion Program, Youth Science and Technology Star Project (grant number: 2020KJXX-028) and the National Program on Key Research and Development Project of China (grant number: 2018YFE0114200).

Declarations

Conflict of interest The authors declare that they have no conflicts of interest.

References

1. Casali PG, Bielack S, Abecassis N et al (2018) Bone sarcomas: ESMO-PaedCan-EURACAN clinical practice guidelines for diagnosis, treatment and follow-up. Ann Oncol. 29:iv79–iv95. https://doi.org/10.1093/annonc/mdy310
2. Alexander JH, Binitie OT, Letson GD, Joyce DM (2021) Osteosarcoma: an evolving understanding of a complex disease. J Am Acad Orthop Surg 29:e993–e1004. https://doi.org/10.5435/jaaos-d-20-00838
3. Harrison DJ, Geller DS, Gill JD, Lewis VO, Gorlick R (2018) Current and future therapeutic approaches for osteosarcoma. Expert Rev Anticancer Ther 18:39–50. https://doi.org/10.1080/14737140.2018.1413939
4. Meazza C, Scanagatta P (2016) Metastatic osteosarcoma: a challenging multidisciplinary treatment. Expert Rev Anticancer Ther 16:543–556. https://doi.org/10.1586/14737140.2016.1168697
5. Huang J, Li J, Zheng S et al (2020) Tumor microenvironment characterization identifies two lung adenocarcinoma subtypes with specific immune and metabolic state. Cancer Sci 111:1876–1886. https://doi.org/10.1111/cas.14390
6. Zhang Y, Zhao Y, Li Q, Wang Y (2021) Macrophages, as a promising strategy to targeted treatment for colorectal cancer metastasis in tumor immune microenvironment. Front Immunol 12:685978. https://doi.org/10.3389/fimmu.2021.685978
7. Mills CD, Lenz LL, Harris RA (2016) A breakthrough: macrophage-directed cancer immunotherapy. Cancer Res 76:513–516. https://doi.org/10.1158/0008-5472.Can-15-1737
8. Li X, Liu R, Su X, Pan Y, Han X, Shao C, Shi Y (2019) Harnessing tumor-associated macrophages as aids for cancer immunotherapy. Mol Cancer 18:177. https://doi.org/10.1186/s12943-019-1102-3
9. Bao X, Shi R, Zhao T, Wang Y, Anastasov N, Rosemann M, Fang W (2021) Integrated analysis of single-cell RNA-seq and bulk RNA-seq unravels tumour heterogeneity plus M2-like tumour-associated macrophage infiltration and aggressiveness in TNBC. Cancer Immunol Immunother 70:189–202. https://doi.org/10.1007/s00262-020-02669-7
10. Nam SH, Kim D, Lee D et al (2018) Lysyl-tRNA synthetase-expressing colon spheroids induce M2 macrophage polarization to promote metastasis. J Clin Invest 128:5034–5055. https://doi.org/10.1172/jci99806
11. Lin Y, Xu J, Lan H (2019) Tumor-associated macrophages in tumor metastasis: biological roles and clinical therapeutic applications. J Hematol Oncol 12:76. https://doi.org/10.1186/s13045-019-0760-3
12. Wu JY, Huang TW, Hsieh YT et al (2020) Cancer-Derived succinate promotes macrophage polarization and cancer metastasis via succinate receptor. Mol Cell 77:213–27.e5. https://doi.org/10.1016/j.molcel.2019.10.023
13. Schmall A, Al-Tamari HM, Herold S et al (2015) Macrophage and cancer cell cross-talk via CCR2 and CX3CR1 is a fundamental mechanism driving lung cancer. Am J Respir Crit Care Med 191:437–447. https://doi.org/10.1164/rccm.201406-1137OC
14. Huang YK, Wang M, Sun Y, Di Costanzo N, Mitchell C, Achuthan A, Hamilton JA, Busuttil RA, Boussioutas A (2019) Macrophage spatial heterogeneity in gastric cancer defined by multiplex immunohistochemistry. Nat Commun 10:3928. https://doi.org/10.1038/s41467-019-11788-4
15. Loyher PL, Hamon P, Laviron M et al (2018) Macrophages of distinct origins contribute to tumor development in the lung. J Exp Med 215:2536–2553. https://doi.org/10.1084/jem.20180534
16. Steenbrugge J, Breyne K, Demeyere K et al (2018) Anti-inflammatory signaling by mammary tumor cells mediates prometastatic macrophage polarization in an innovative intraductal mouse model for triple-negative breast cancer. J Exp Clin Cancer Res 37:191. https://doi.org/10.1186/s13046-018-0860-x
17. Chen Y, Zhang S, Wang Q, Zhang X (2017) Tumor-recruited M2 macrophages promote gastric and breast cancer metastasis via M2 macrophage-secreted CHI3L1 protein. J Hematol Oncol 10:36. https://doi.org/10.1186/s13045-017-0408-0
18. Huang R, Wang S, Wang N et al (2020) CCL5 derived from tumor-associated macrophages promotes prostate cancer stem cells and metastasis via activating β-catenin/STAT3 signaling. Cell Death Dis 11:234. https://doi.org/10.1038/s41419-020-2435-y
19. Liu C, Yao Z, Wang J et al (2020) Macrophage-derived CCL5 facilitates immune escape of colorectal cancer cells via the p65/STAT3-CSN5-PD-L1 pathway. Cell Death Differ 27:1765–1781. https://doi.org/10.1038/s41418-019-0460-0
20. Wang N, Liu W, Zheng Y et al (2018) CXCL1 derived from tumor-associated macrophages promotes breast cancer metastasis via activating NF-κB/SOX4 signaling. Cell Death Dis 9:880. https://doi.org/10.1038/s41419-018-0876-3
21. Wang D, Sun H, Wei J, Cen B, DuBois RN (2017) CXCL1 Is Critical for Premetastatic niche formation and metastasis in colorectal cancer. Cancer Res 77:3655–3665. https://doi.org/10.1158/0008-5472.Can-16-3199
22. Li R, Zhou R, Wang H et al (2019) Gut microbiota-stimulated cathepsin K secretion mediates TLR4-dependent M2 macrophage polarization and promotes tumor metastasis in colorectal cancer. Cell Death Differ 26:2447–2463. https://doi.org/10.1038/s41418-019-0312-y
23. Trikha P, Sharma N, Pena C et al (2016) E2f3 in tumor macrophages promotes lung metastasis. Oncogene 35:3636–3646. https://doi.org/10.1038/onc.2015.429
24. Mi X, Xu R, Hong S, Xu T, Zhang W, Liu M (2020) M2 Macrophage-derived exosomal lncRNA AFAP1-AS1 and MicroRNA-26a affect cell migration and metastasis in esophageal cancer. Mol Therapy Nucleic acids 22:779–790. https://doi.org/10.1016/j.omtn.2020.09.035
25. Wu J, Gao W, Tang Q et al (2021) M2 macrophage-derived exosomes facilitate HCC metastasis by transferring αM β2 integrin to tumor cells. Hepatology (Baltimore, Md.) 73:1365–80. https://doi.org/10.1002/hep.31432
26. Lan J, Sun L, Xu F et al (2019) M2 Macrophage-Derived Exosomes Promote Cell Migration and Invasion in Colon Cancer. Cancer Res 79:146–158. https://doi.org/10.1158/0008-5472.Can-18-0014
27. Wei C, Yang C, Wang S, Shi D, Zhang C, Lin X, Liu Q, Dou R, Xiong B (2019) Crosstalk between cancer cells and tumor associated macrophages is required for mesenchymal circulating tumor cell-mediated colorectal cancer metastasis. Mol Cancer 18:64. https://doi.org/10.1186/s12943-019-0976-4
28. Geng Y, Fan J, Chen L et al (2021) A notch-dependent inflammatory feedback circuit between macrophages and cancer cells regulates pancreatic cancer metastasis. Cancer Res 81:64–76. https://doi.org/10.1158/0008-5472.Can-20-0256
29. Walens A, DiMarco AV, Lupo R, Kroger BR, Damrauer JS, Alvarez JV (2019) CCL5 promotes breast cancer recurrence through macrophage recruitment in residual tumors. eLife. https://doi.org/10.7554/eLife.43653
30. Seoane S, Martinez-Ordoñez A, Eiro N et al (2019) POU1F1 transcription factor promotes breast cancer metastasis via recruitment

and polarization of macrophages. J Pathol 249:381–394. https://doi.org/10.1002/path.5324
31. Li J, Zhao C, Li Y et al (2022) Osteosarcoma exocytosis of soluble LGALS3BP mediates macrophages toward a tumoricidal phenotype. Cancer Lett 528:1–15. https://doi.org/10.1016/j.canlet.2021.12.023
32. Verrier S, Peroglio M, Voisard C, Lechmann B, Alini M (2011) The osteogenic differentiation of human osteoprogenitor cells on Anodic-Plasma-Chemical treated Ti6Al7Nb. Biomaterials 32:672–680. https://doi.org/10.1016/j.biomaterials.2010.09.028
33. Zhang P, Li J (2021) Down-regulation of circular RNA hsa_circ_0007534 suppresses cell growth by regulating miR-219a-5p/SOX5 axis in osteosarcoma. J Bone Oncol 27:100349. https://doi.org/10.1016/j.jbo.2021.100349
34. Liang JQ, Zhou ZT, Bo L, Tan HN, Hu JH, Tan MS (2021) Phosphoglycerate kinase 1 silencing by a novel microRNA microRNA-4523 protects human osteoblasts from dexamethasone through activation of Nrf2 signaling cascade. Cell Death Dis 12:964. https://doi.org/10.1038/s41419-021-04250-1
35. Kessenbrock K, Plaks V, Werb Z (2010) Matrix metalloproteinases: regulators of the tumor microenvironment. Cell 141:52–67. https://doi.org/10.1016/j.cell.2010.03.015
36. Lin EY, Li JF, Gnatovskiy L, Deng Y, Zhu L, Grzesik DA, Qian H, Xue XN, Pollard JW (2006) Macrophages regulate the angiogenic switch in a mouse model of breast cancer. Cancer Res 66:11238–11246. https://doi.org/10.1158/0008-5472.Can-06-1278
37. Qian B, Deng Y, Im JH, Muschel RJ, Zou Y, Li J, Lang RA, Pollard JW (2009) A distinct macrophage population mediates metastatic breast cancer cell extravasation, establishment and growth. PLoS ONE 4:e6562. https://doi.org/10.1371/journal.pone.0006562
38. Maimon A, Levi-Yahid V, Ben-Meir K et al (2021) Myeloid cell-derived PROS1 inhibits tumor metastasis by regulating inflammatory and immune responses via IL-10. J Clin Invest. https://doi.org/10.1172/jci126089
39. Chen YQ, Li PC, Pan N et al (2019) Tumor-released autophagosomes induces CD4+ T cell-mediated immunosuppression via a TLR2-IL-6 cascade. J Immunother Cancer 7:178. https://doi.org/10.1186/s40425-019-0646-5
40. Lee CC, Lin JC, Hwang WL, Kuo YJ, Chen HK, Tai SK, Lin CC, Yang MH (2018) Macrophage-secreted interleukin-35 regulates cancer cell plasticity to facilitate metastatic colonization. Nat Commun 9:3763. https://doi.org/10.1038/s41467-018-06268-0
41. Balkwill F, Mantovani A (2001) Inflammation and cancer: back to Virchow? Lancet 357:539–545. https://doi.org/10.1016/s0140-6736(00)04046-0
42. Qian BZ, Li J, Zhang H, Kitamura T, Zhang J, Campion LR, Kaiser EA, Snyder LA, Pollard JW (2011) CCL2 recruits inflammatory monocytes to facilitate breast-tumour metastasis. Nature 475:222–225. https://doi.org/10.1038/nature10138
43. Uehara S, Song K, Farber JM, Love PE (2002) Characterization of CCR9 expression and CCL25/thymus-expressed chemokine responsiveness during T cell development: CD3(high)CD69+ thymocytes and gammadeltaTCR+ thymocytes preferentially respond to CCL25. J Immunol 168:134–142. https://doi.org/10.4049/jimmunol.168.1.134
44. Spinnen J, Fröhlich K, Sinner N, Stolk M, Ringe J, Shopperly L, Sittinger M, Dehne T, Seifert M (2021) Therapies with CCL25 require controlled release via microparticles to avoid strong inflammatory reactions. J Nanobiotechnol 19:83. https://doi.org/10.1186/s12951-021-00830-7
45. Johnson-Holiday C, Singh R, Johnson E, Singh S, Stockard CR, Grizzle WE, Lillard JW (2011) CCL25 mediates migration, invasion and matrix metalloproteinase expression by breast cancer cells in a CCR9-dependent fashion. Int J Oncol 38:1279–1285. https://doi.org/10.3892/ijo.2011.953
46. Niu Y, Tang D, Fan L, Gao W, Lin H (2020) CCL25 promotes the migration and invasion of non-small cell lung cancer cells by regulating VEGF and MMPs in a CCR9-dependent manner. Exp Ther Med 19:3571–3580. https://doi.org/10.3892/etm.2020.8635
47. Morikawa R, Nakamoto N, Amiya T et al (2021) Role of CC chemokine receptor 9 in the progression of murine and human non-alcoholic steatohepatitis. J Hepatol 74:511–521. https://doi.org/10.1016/j.jhep.2020.09.033
48. Wurbel MA, McIntire MG, Dwyer P, Fiebiger E (2011) CCL25/CCR9 interactions regulate large intestinal inflammation in a murine model of acute colitis. PLoS One 6:e16442. https://doi.org/10.1371/journal.pone.0016442
49. Umar S, Palasiewicz K, Van Raemdonck K et al (2021) CCL25 and CCR9 is a unique pathway that potentiates pannus formation by remodeling RA macrophages into mature osteoclasts. Eur J Immunol 51:903–914. https://doi.org/10.1002/eji.202048681
50. Jacquelot N, Enot DP, Flament C et al (2016) Chemokine receptor patterns in lymphocytes mirror metastatic spreading in melanoma. J Clin Invest 126:921–937. https://doi.org/10.1172/jci80071
51. Cortés M, Sanchez-Moral L, de Barrios O et al (2017) Tumor-associated macrophages (TAMs) depend on ZEB1 for their cancer-promoting roles. EMBO J 36:3336–3355. https://doi.org/10.15252/embj.201797345
52. Chen XJ, Deng YR, Wang ZC et al (2019) Hypoxia-induced ZEB1 promotes cervical cancer progression via CCL8-dependent tumour-associated macrophage recruitment. Cell Death Dis 10:508. https://doi.org/10.1038/s41419-019-1748-1
53. Ma L, Yu L, Jiang BC et al (2021) ZNF382 controls mouse neuropathic pain via silencer-based epigenetic inhibition of Cxcl13 in DRG neurons. J Exp Med. https://doi.org/10.1084/jem.20210920
54. Jen J, Wang YC (2016) Zinc finger proteins in cancer progression. J Biomed Sci 23:53. https://doi.org/10.1186/s12929-016-0269-9
55. Cheng Y, Geng H, Cheng SH et al (2010) KRAB zinc finger protein ZNF382 is a proapoptotic tumor suppressor that represses multiple oncogenes and is commonly silenced in multiple carcinomas. Cancer Res 70:6516–6526. https://doi.org/10.1158/0008-5472.Can-09-4566
56. Kusic DM, Roberts WN, Jarvis JP, Zhang P, Scheinfeldt LB, Rajula KD, Brenner R, Dempsey MP, Zajic SC (2020) rs11670527 Upstream of ZNF264 Associated with Body Mass Index in the Coriell Personalized Medicine Collaborative. Mil Med 185:649–655. https://doi.org/10.1093/milmed/usz216
57. Kaplan RN, Riba RD, Zacharoulis S et al (2005) VEGFR1-positive haematopoietic bone marrow progenitors initiate the pre-metastatic niche. Nature 438:820–827. https://doi.org/10.1038/nature04186
58. Zhang M, Song C, Li G, Chen L, Ma R, Yu X, Gong P, Wang X (2020) Transplantation of umbilical cord blood mononuclear cells attenuates the expression of IL-1β via the TLR4/NF-κB pathway in hypoxic-ischemic neonatal rats. J Neurorestoratology 8:122–130. https://doi.org/10.26599/jnr.2020.9040015
59. Helm O, Held-Feindt J, Grage-Griebenow E et al (2014) Tumor-associated macrophages exhibit pro- and anti-inflammatory properties by which they impact on pancreatic tumorigenesis. Int J Cancer 135:843–861. https://doi.org/10.1002/ijc.28736
60. Lee S, Heinrich EL, Li L et al (2015) CCR9-mediated signaling through β-catenin and identification of a novel CCR9 antagonist. Mol Oncol 9:1599–1611. https://doi.org/10.1016/j.molonc.2015.04.012